Journal of Autonomous Intelligence (2022) Volume 5 Issue 1.
doi: 10.32629/jai.v5i1.509

Original Research Article

Translational Speed Control and Positioning of Precision Agricultural Robot

Leonardo Enrique Solaque Guzmán[1], Guillermo Sánchez Herrera[2], Adriana Riveros Guevara[3]

[1] Doctor en Ingeniería, Docente de planta, Leonardo.

[2] Ingeniero Mecatrónico, Asistente de investigación

[3] Magister en Mecatrónica, Docente ocasional

ABSTRACT

All kinds of agricultural labor may lead to farmers' fatigue or disease. To help accomplish these tasks, robotics is used as a possibility to minimize the above inconvenience. With this in mind, the Military University of New Granada designed and built a robot called CERES, which is responsible for removing weeds, spraying, etc. In order for CERES to move in the crop along the required path, it must be ensured that the robot moves at a specific translational speed and direction, which is ensured by using the controller. This paper introduces the use of SSV (steady state value) criterion and the control signal allowed by the robot hardware, designs and implements a PID controller for tracking the linear speed and direction and ensuring that the stability time is met when the error tends to zero.

Keywords: *Agricultural Robots; Control; Modeling; Robotics*

ARTICLE INFO

Received: Feb 27, 2022
Accepted: Apr 19, 2022
Available online: May 5, 2022

***CORRESPONDING AUTHOR**

Leonardo Enrique Solaque Guzmán
solaque@unimilitar.edu.co;

CITATION

Solaque Guzmán LE, Sánchez Herrera G, Riveros Guevara A. Translational speed control and positioning of precision agricultural robot. Journal of Autonomous Intelligence 2022; 5(1): 85-94. doi: 10.32629/jai.v5i1.509

1. Introduction

It is estimated that the population growth of 3 trillion by 2025[1] poses a major challenge to the agricultural sector. Over the past few decades, the increase of agricultural productivity has led to a decline in the proportion of malnutrition in the world population[2]. Crop intensification, mechanization and automation are crucial to agricultural productivity by improving efficiency, accuracy and reliability[3]. The use of intelligent machinery can significantly improve the yield of traditional crops, which are currently operated by farmers manually[4]. Agricultural robots need skilled workers and technical equipment, which is very attractive to the new generation, thus slowing down the continuous growth of the average age of farmers[5]. Robot technology has made great progress in industry, but in complex environment and agricultural environment, the brightness, temperature and humidity change greatly, so a strong system is needed to support agricultural work safely.

Mobile robots, especially autonomous robots, allow real-time crop selection and action without human intervention; Its application in repetitive work requiring accuracy is very important. However, due to uncertainties and unpredictable environmental conditions, 100% autonomous vehicles are still under development in complex and unstructured environments[6]. To this end, GIDAM team is developing an agricultural robot called "CERES" for precision agriculture tasks. This structure has a weeding system, a centralized solid nutrition application system and a fumigation system designed to meet environmental

standards[7].

In order to complete the main farming care tasks (weeding, spraying and fertilization), the robot must meet the requirements of mobility and operability in order to complete these tasks in the whole farming process. The displacement is controlled by the low-level orientation and speed controller based on the platform state, which is measured by the sensors available on the platform. A robot was developed in **Figure 8**. Each robot has four driving wheels and steering wheels, which are used to accurately sow wheat, and the effective sowing rate is more than 90%. A directional control system, as shown in **Figure 9**, is used to navigate the robot through markers in the greenhouse. Autonomy was also tested through the integration of commercial vehicles. A golf cart (including navigation sensors and cameras) was modified to realize autonomous navigation on crops and avoid obstacles as shown in **Figure 10**.

The second section introduces the motion system of CERES robot, establishes the dynamic model from Newton Euler and Euler Lagrange methods, designs the PID control law and applies it to the robot. Section 3 presents the results of simulation and actual tests. This paper summarizes the work of precision agriculture in the future.

2. Materials and methods

In this section, the kinematics and dynamics of CERES robot are modeled, the control laws are proposed, and the implementation of these control laws on the actual prototype is introduced in detail.

CERES platform is designed in GIDAM (electromechanical application research and development group) of electromechanical engineering project of New Granada military university. It aims to improve the quality of life of farmers and contribute to the process of precision agriculture. **Figure 1** shows the CERES platform.

Figure 1. CERES pictures: Electric differential tractor (48V), carrying capacity of 100 kg solid fertilizer, 20 liters fumigation and weeding system.

2.1 Kinematic modeling

In the motion model, according to the local motion of the structure—frame robot (R_b), we seek to reference the platform motion to the general or global frames (R_o)[11,12]. **Figure 2** shows a robot in three-dimensional space with respective coordinate systems.

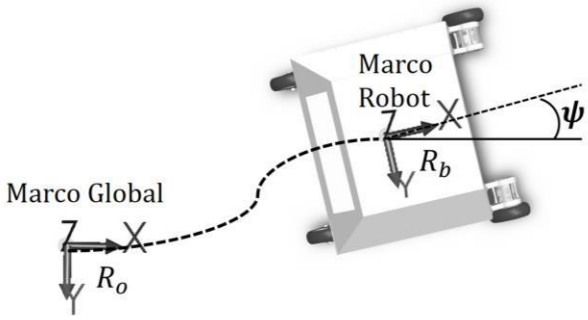

Figure 2. Global frame, local frame-robot and path connecting global frame and local frame.

Assuming that the robot moves at the speed u of translation and ω of rotation in the local frame (R_b), the speed reflected in the global coordinate system (R_o) can be found. P represents the position (x,y) and direction (ψ) of the robot in space (R_o), it can be found that the relationship between the speeds in each reference frame is given by equation 1: transformation from (R_o) to (R_b), where $s\varphi = \sin(\psi)$ and $c\varphi = \cos(\psi)$.

$$\dot{p} = \begin{bmatrix} \dot{x} \\ \dot{y} \\ \dot{\psi} \end{bmatrix} = \begin{bmatrix} c\psi & 0 \\ s\psi & 0 \\ 0 & 1 \end{bmatrix} \begin{bmatrix} u \\ \omega \end{bmatrix} = R_o^b \begin{bmatrix} u \\ \omega \end{bmatrix} \tag{1}$$

It is worth noting that the speed in R_b and the speed in the whole system are determined by $\begin{bmatrix} u \\ \omega \end{bmatrix} = (R_o^b)^{-1}\dot{P}$. It is worth noting that the system imposes a nonholonomic constraint represented by the $\dot{x}s\varphi = \dot{y}c\varphi$ equation.

2.2 Newton Euler and Euler Lagrange dynamic modeling

Newton-Euler's modeling theory is based on the physical principle of the element. The system dynamics consists of equation 2.

$$M\dot{x} = \sum F$$
$$I\ddot{\varphi} = \sum \tau \tag{2}$$

Among them M is the mass of the robot, I is the inertia of the system, F is the force and τ is the moment of the robot, which are provided by the contact between each rim and the ground (see **Figure 3**). Where x is translation displacement and φ rotation displacement or direction.

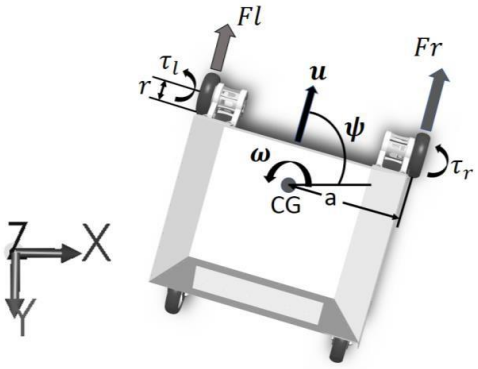

Figure 3. The system model is established by system force and system speed.

Figure 3 shows the center of gravity CG, the sum of all forces and moments. Therefore, the force generated by each rim is proportional to the torque generated by each motor ($Fr = \tau$, where r is the radius of rim). Therefore, CG equation 3 gives the physical relationship related to rotational motion.

$$v_r = v_{CG} + a\omega$$
$$v_1 = v_{CG} - a\omega$$

Therefore:

$$v_{CG} = u = \frac{1}{2}(v_r + v_1)$$
$$\dot{\psi} = \omega = \frac{1}{2a}(v_r - v_1) \tag{3}$$

Where, $v_r = r\theta_r$ and $v_1 = r\theta_1$ is the tangent speed of the left and right rims respectively, and a is the distance measured from the rim to the center of gravity.

Euler-Lagrange theory allows the establishment of dynamic ($L = K - P$) equations on Lagrangiano, which are composed of kinetic energy K and potential energy P. This method usually supplements or supplements Newton-Euler model. In this case, it allows the completion of dynamics related to the structural geometry and its dimensions (data measured in the physical system or CAD model). Assuming the same friction coefficient and inertia due to the rim engine combination on the two rims, equation 4 is used to determine the system dynamics through the Euler-Lagrange model.

$$\frac{d}{dt}\left(\frac{\partial L}{\partial \dot{q}}\right) - \frac{\partial L}{\partial q} = \sum F \tag{4}$$

The total kinetic energy of the structure is defined as the sum of the single input of the structure under translation ($k_1 = \frac{1}{2}Mv_{CG}^2$) and rotation ($k_2 = \frac{1}{2}I_{CG}\omega^2$), the rim kinetic energy ($k_3 = \frac{1}{2}I_{llanta}\dot{\theta}_r^2 + \frac{1}{2}I_{llanta}\dot{\theta}_1^2$) and zero potential energy ($P = 0$), and the Lagrange equation is $L = k_1 + k_2 + k_3$. After mathematical operation and application of equation 4, the dynamics of CERES robot is described in equation 5.

$$\beta_{11}\ddot{\theta}_r + \beta_{12}\ddot{\theta}_l + \beta\dot{\theta}_r = \tau_r$$
$$\beta_{21}\ddot{\theta}_r + \beta_{22}\ddot{\theta}_l + \beta\dot{\theta}_l = \tau_l \tag{5}$$

Of which:

$$\beta_{11} = \beta_{22} = \left[\frac{Mr^2}{4} + \frac{I_{CG}r^2}{4a^2} + I_{llanta}\right]$$

$$\beta_{12} = \beta_{21} = \left[\frac{Mr^2}{4} - \frac{I_{CG}r^2}{8a^2}\right]$$

In addition, β is a coefficient related to rim friction and the terrain of robot movement. The τ_r and τ_l is generated by the engine. Due to the 48 volt power drive vector 300 and 5KW HPM5000B engine of manufacturer golden motors, the inherent dynamics cannot be found immediately[13]. As described in subsection 2.3, the integrity of the model is caused by factors such as insufficient engine characteristic information or power handle (driver) information. Dynamic identification from input voltage to power handle, torque to each wheel and/or tangential speed is considered, as described in subsection 2.3.

It is worth noting that the coefficient values related to the prototype and used for simulation are determined from robot CAD (**Table 1**).

Table 1. System coefficient

Description of	Parameter meter	Courage
Quality	M	530Kg
Inertia	I_{CG}	47*10^9 Kg*M2
Inertia rim	I_{llanta}	219*10^6 Kg*M2
Distance from center of gravity to rim (transverse)	a	1.2m
Rim radius	r	0.28m

2.3 Dynamic identification of power handle and motor at tangential speed

According to the principle that the input voltage (V_{in_i}) of the DC motor is directly proportional to the current flowing through it, and the current is directly proportional to the torque (τ_i) generated by the DC motor. The input voltage driven by 5KW HPM5000B motor power can be set in proportion to the generated torque. Therefore, the rotation speed is set by the signal input to the motor. A motor dynamic identification model based on CERES platform is proposed.

Generally, the little knowledge or description of the dynamics related to the engine and power handle is not easy to determine from the manufacturer's information, so it is decided to identify the dynamics and integrate it into the model of equation 5.

According to the parameter identification technology, it is decided to place the input stage on the system from the engine power handle to the tangential speed ($V_T = r\theta$). In this case, the parametric least squares adaptive algorithm is assumed[14-16].

Then the pseudo-random signal (PRBS pseudo-random binary sequence) is applied to the model, and the data is obtained from the system output, and transmitted to the parameter estimation algorithm, such as recursive least squares (RLS), so as to produce a fully representative first-order system (similarity is 94%). Taking the tire angular velocity (rad/s) equation 6 as the function of input voltage (V), the relationship between left and right engine models is established.

$$V_{T_r}(s) = r\dot{\theta}_r(s) = \frac{K_r V_{in\_r}}{\eta_r s + 1}$$

$$V_{T_l}(s) = r\dot{\theta}_l(s) = \frac{K_l V_{in\_l}}{\eta_l s + 1} \quad (6)$$

In the case, K_i is the system gain, V_{in_i} is the voltage input to the power processor, and η_i is the system time constant. The determined values are shown in **Table 2**.

Table 2. Motor parameter identification

Parameter meter	Courage
K_r	35.8
K_l	42.1
η_r	0.94
η_l	1.08

2.4 Control law design

For the models described in equations 5 and 6, the main dynamics related to the platform geometry must obey the terms β_{11} and β_{12}, because the terms β_{12} and β_{21} account for approximately 13% the total value. This shows that the speed of each rim can be assumed without dynamic coupling with the other rim, all within the speed range at which the structure will move to linear and angular speeds).

This allows equations 5 and 6 to be rewritten as shown in equation 7, showing independent dynamics.

$$(\beta_{11}s+\beta)\omega_r = \frac{K_r V_{in\_r}}{\eta_r s+1}$$

$$(\beta_{22}s+\beta)\omega_l = \frac{K_{Tl} V_{in\_l}}{\eta_l s+1} \tag{7}$$

This K_{Tr} and K_{Tl} include all gains of subsystems or unmodeled gains.

Starting from equation 7, a PID control is proposed to stabilize the translation speed and direction (remember, they are a function of rim angular speed). Based on a Hurwitz polynomial, it establishes the required closed-loop dynamics (respecting the natural dynamics of the system, so that it will not exert great pressure on the control signal and will not be transmitted to the motor). Equation 8 shows the proposed controller.

$$u_u(t) = k_{pu}e_u(t) + k_{du}\frac{de_u(t)}{dt} + k_{iu}\int e_u(t)dt$$

$$u_\Psi(t) = k_{pd}e_\psi(t) + k_{dd}\frac{de_\psi(t)}{dt} + k_{id}\int e_\psi(t)dt \tag{8}$$

In the equation, $e_u(t) = u_d(t) - u(t)$ and $e_\psi(t) = \psi_d(t) - \psi(t)$, where u_d and ψ_d are the expected values of translation speed and direction respectively. It should be remembered that the measured translational speed is $u = v_{CG}$.

The values of controller constants are shown in **Table 3**.

Table 3. Gain controller

Gain	Courage
K_{pd} (proportional direction)	0.8
K_{id} (integration direction)	0.4
K_{dd} (derived address)	0.0
K_{pu} (proportional speed)	1.1
K_{iu} (speed integral)	0.65
K_{du} (velocity derivative)	0.0

According to the relationship given in Equations 3, 6 and 8, the voltage that must be reached by each motor is determined.

For the test of the control device, the equations related to kinematics, dynamics and dynamic control have been programmed, as shown in **Figure 4**.

It is worth noting that the design is carried out in the continuous time domain and the implementation is carried out in the discrete time domain. Discretization starts from selecting the sampling time of the system ($tm = 1/20$), and takes the system stability within 5s and the response time as 1s. Under the condition that the response time is 20 times of the sampling time, a working frequency is selected when calculating the 20Hz control signal. Because the discretization method of "zero order ZoH-holder" has balance in time and frequency response, it is selected to realize the discretization of control law.

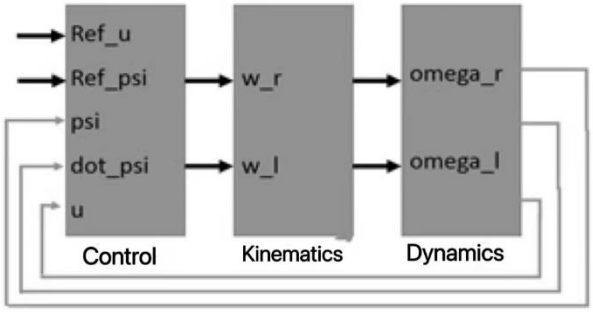

Figure 4. Schematic diagram of model test and controller simulation.

2.5 Put the controller into operation

The integration and testing of the controller is carried out in the modular robot operating system (ROS) environment, which allows the modularization of different sensors and actuators.

ROS provides a communication layer running on Linux operating system and heterogeneous computer clusters (for example: Computer and one or more embedded systems). One of its most relevant functions is to provide peer-to-peer communication, which can be programmed in C++ and python, and run programs from different languages in the same project. ROS has tools to easily view, monitor the runtime and integrate different components. Finally, ROS is open-source software under the BSD license and has a wide community, which helps to correct errors and support[17]. For more information, there are a large number of official tutorials on *www.ros.org*.

ROS master node can run on embedded system

or computer and connect to hardware through Ethernet, serial or other communication systems. Devices on the network can obtain information, process information and publish operations, all of which can be performed using connected hardware or software nodes.

In the platform control scheme, there is a scheduler and a trajectory tracking control, which is called high-level control. This provides a reference for translational speed and directional control, which is called low level control. **Figure 5** shows the control scheme considering trajectory tracking. Therefore, the focus of this paper is to realize the bottom control, which is programmed as an Arduino mega, which is connected to the host computer running the ROS master node through serial communication. This section describes the hardware and data flow used to test the designed controller.

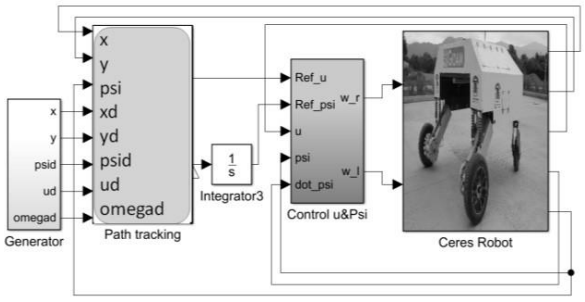

Figure 5. CERES platform monitoring scheme.

Figure 6 shows the hardware used for the experiment. The actuator of the control system is the motor of CERES robot, which is connected to the rim of RIN 14 of traditional automobile. The sensor corresponds to IMU spatial navigation, which integrates GPS and allows to understand the state of the robot.

The processing is performed by a laptop running the ROS master node and an Arduino mega, which allows the command to be received through the ROS message and sends the control signal (voltage) to the motor. For this purpose, the optical coupling phase is performed between the motor power processing program receiving the control signal and Arduino. In order to realize the displacement of the robot before and after the experiment, a wireless control is added to make the manual displacement of CERES.

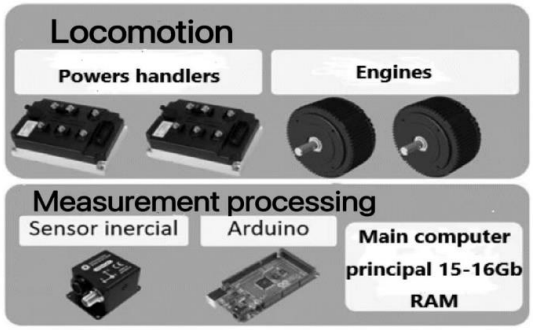

Figure 6. Hardware used.

Figure 7 shows the communication speed of the main system elements and transmission variables. This is achieved by programming the ROS node, which runs on the computer and obtains information from the IMU (IMU implements the manufacturer's tuned Kalman filter), which is preprocessed to send to the node related to Arduino. Arduino receives information from reference and current measurements to calculate analog signals and send them to the power processor, publishing these values to the master node for data recording.

In the experiment, the robot is moved to a large range and sends step-by-step commands from the radio control or from the ROS node issuing these preprogrammed commands at angular position and linear speed.

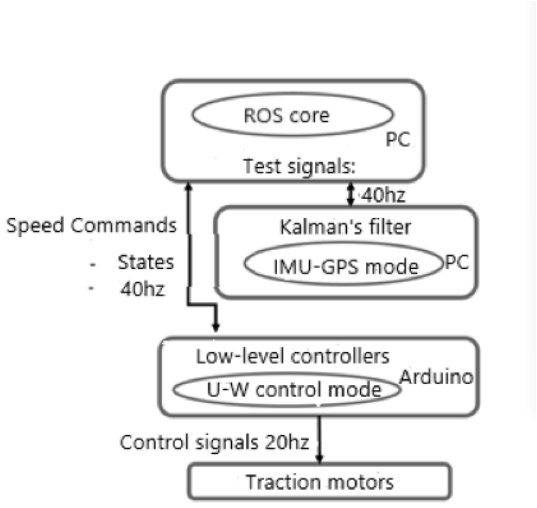

Figure 7. Communication scheme between shipboard computer and programmable operating system in embedded system.

3. Result

This section describes the response curve of the simulation system and the same control implemented on the prototype. The design criterion of the control is realized on the basis that the steady-state error is close to zero ($e_{ss} = 0$), the establishment time is similar to that of the open-loop system (using SSV criterion) and the response time close to the critical damping ($\xi = 1$).

3.1 Simulation results

Figure 8 and **Figure 9** show the simulation of the vehicle at translational speed $u_d = 0.5m/s$ and direction $\psi_d = \frac{-\pi}{10} rad$. **Figure 8** shows that the speed and direction output signals approach the reference step when approaching the open loop. In this case, the linear speed is close to 2.5s and the direction time is more than 8s. It is worth noting that in determining these times, the settlement standard (SSV) is used, which is determined near the final value. Within 10% in **Figure 9**, it can be observed that the control signal (for right engine and left engine) is within the allowable range of engine power processor.

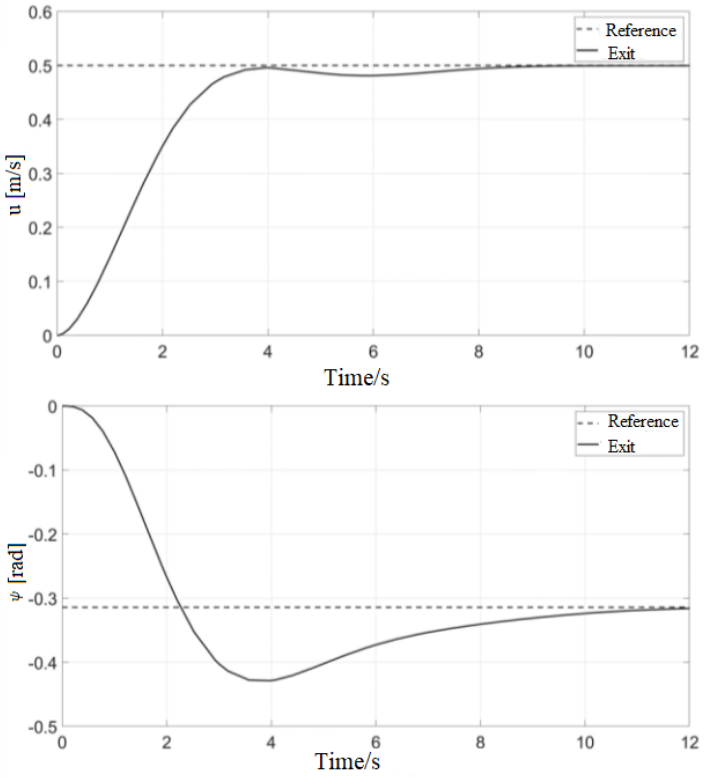

Figure 8. Tracking speed and direction reference-simulation test

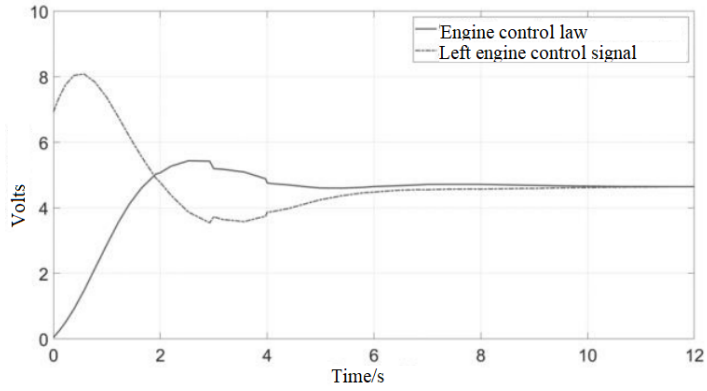

Figure 9. The control signal is consistent with the voltage allowed by the power controller - simulation test.

3.2 Experimental results

After completing the programming of point electronics and control algorithm, we carried out the same experiment as the reference signal used in the simulation.

On the premise of not losing the universality of the test, the test was carried out on the cement surface. This is supported on the basis that there is a measurement signal with a central inertial sensor fusion and Kalman filter.

Figure 10 shows the tracking of references, extracting the output from the information provided by the ship's inertial Center (speed and direction) to prove the tracking of the required signal.

The translation speed stability time of the actual system is close to 2s. The direction of the robot reaches the benchmark in about 6s.

These times are close to simulation experiments. These differences can be attributed to the slower dynamics in the recognition process, which is actually faster dynamics.

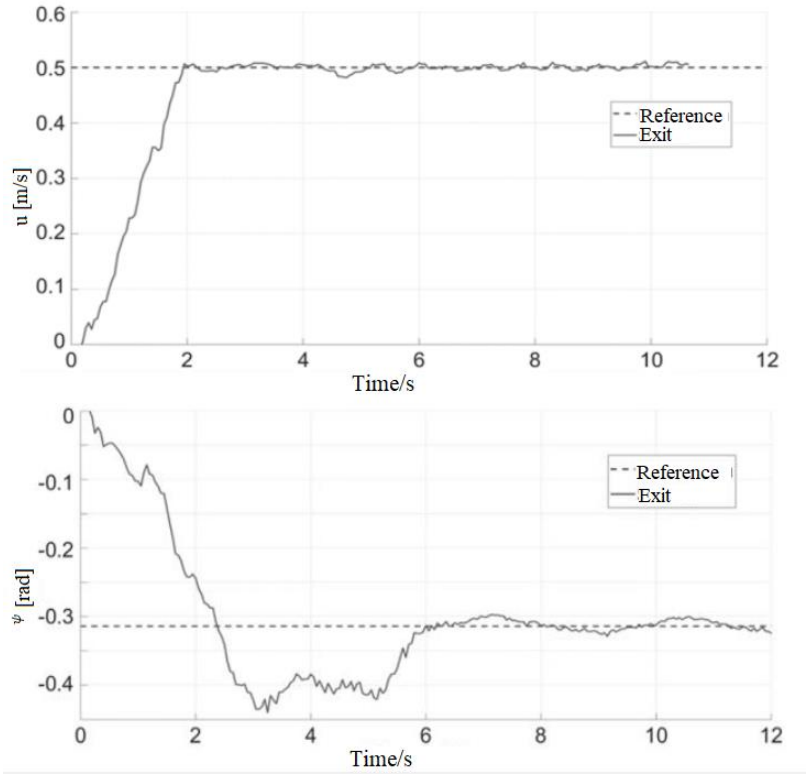

Figure 10. Tracking speed and direction reference-actual test.

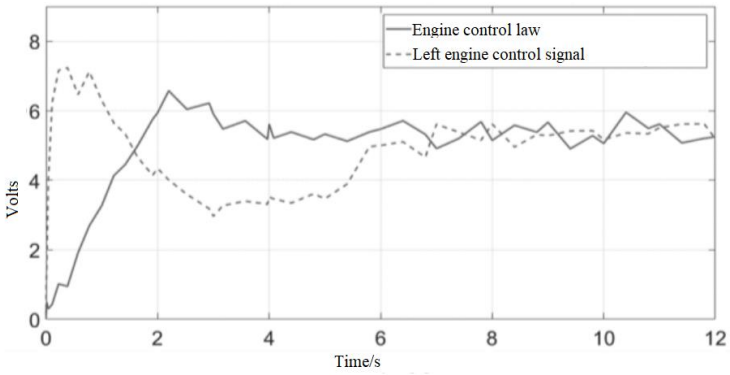

Figure 11. The control signal is consistent with the voltage allowed by the power manager-actual test.

Figure 11 shows the voltage applied to the motor power processor. Their response is similar to the dynamic simulation results. The initial value varies with the conditions in the simulated environment and the initial conditions in the actual environment.

In conclusion, the assumption of developing control and coding in robot programming environment (such as ROS) ensures acceptable performance at the level of dynamic similarity between simulation and actual results.

4. Conclusion

Under the guidance of supporting agricultural labor to improve production efficiency and reduce farmers' risks, the technical input of agricultural comprehensive enterprises is a framework. Therefore, by implementing the platform described in this paper, robot technology opens up an action field for agricultural industry.

In order to seek the autonomy of autonomous robot platform CERES, its modeling is studied from the perspective of kinematics and dynamics. It is found that some parts of the model are not easy to be determined from the CAD structure or the information of the component manufacturer installed on the robot. Therefore, the use of identification technology can supplement the mathematical model to determine the dynamic model that cannot be determined directly in theory.

In the context of finding relevant models, reduce the complexity of the controller, and consider the limitations of platform motion. According to the actual displacement of the robot, a model that can adequately represent CERES dynamics can be established, from which proportional, integral and derivative control can be designed, calculated from the traditional PID design, and the stability can be ensured according to Hurwitz theory.

The simulation results verify the actual allowable value of the structure. Therefore, the provided tests show that the reference tracking is consistent with the translation speed and orientation within the allowable value of the motor power manipulator and the inherent dynamic range of the actual robot.

According to the stability analysis of SSV standard, the design and test of the control device, whether in the simulation or in the actual prototype, show that it is stable within the open-loop time provided by the system, and use the control signal according to the restrictions supported by the motor power controller.

Although the test is carried out on the cement surface, it can be determined that the signal fed back by the controller is provided by an inertial center, which performs sensor fusion based on Kalman filter. This minimizes mileage measurement problems, which usually occur in structures similar to CERES structures and are extrapolated to sliding surfaces.

The integration of the development platform is realized on the basis of modularization. It is integrated through threads dedicated to reading sensors, calculating control signals and other threads dedicated to dialogue with robot actuators, all of which are programmed in ROS environment.

In agricultural work, the next step in the CERES platform upgrade is to develop controls that track a given path, that is, close controls in a hierarchy higher than the controls shown here (low-level controls).

Conflict of interest

The authors declare that they have no conflict of interest.

Acknowledgements

This work was supported by the INV-ING-2637 project entitled "autonomous methods for precision agricultural robot platforms", and was funded by the research department of the New Granada military university in Bogota, Colombia.

References

1. World Population Prospects—Population Division—United Nations. population [Internet]. 2018. Available from: https://population.un.org/wpp/.
2. Goal 2: Zero hunger UNDP [Internet]. 2018 [cited 2018 Sep 29]. Available from: http://www.undp.org/content/undp/en/home/sustainable-development-goals/goal-2-zero-hunger.html. HTML document.
3. Zhang Q. Opportunity of robotics in specialty crop production. IFAC Proceedings 2013; 46(4): 38-39.
4. Xia C, Wang L, Chung B, *et al.* In situ 3D segmentation of individual plant leaves using a RGB-D camera for agricultural automation. Sensor 2015;

15(8): 63-79.

5. Aravind KR, Raja P, Perez-Ruiz M. Task-based agricultural mobile robots in arable farming: A review. Spanish Journal of Agricultural Research 2017; 15(1): e02R01-e02R01.
6. -Xiang R, Jiang H, Ying Y. Recognition of clustered tomatoes based on binocular stereo vision. Computers and Electronics in Agriculture 2014; 106: 75-90.
7. European Parliament. Provisional agreement resulting from interinstitutional negotiations [Internet]. 2017 [cited 2018 Sep 29] Available from: http://www.europarl.europa.eu/RegData/commissio-ns/agri/inag/2017/11-21/AGRI_AG%282017%29613578_EN.
8. Haibo L, Shuliang D, Zunmin L, *et al.* Study and experiment on a wheat precision seeding robot. Journal of Robotics 2015; 1-9.
9. Gat G, Gan-Mor S, Degani A. Stable and robust vehicle steering control using an overhead guide in greenhouse tasks. Computers and Electronics in Agriculture 2016; 121: 234-244.
10. Ball D, Upcroft B, Wyeth G. Vision-based obstacle detection and navigation for an agricultural robot. Journal of Field Robotics 2016; 33(8): 1107-1130. doi: doi:10.1002/rob.21644.
11. Siegwart R, Nourbakhsh I. Introduction to autonomous mobile robots. 2nd ed. Cambridge: MIT Press; 2016.
12. Tzafestas S. Mobile robot control and navigation: A global overview. Journal of Intelligent & Robotic Systems 2018; 91(1): 35-58.
13. Golden motor Canada [Internet]. [cited 2018 Sep 29].Available from: https://www.goldenmotor.ca/.
14. Landau I. Digital control systems. London: Springer; 2007.
15. Ljung L. System identification. 2nd ed. New Jersey: Prentice Hall PTR; 2012.
16. Astrom K, Wittenmark B. Computer-controlled Systems. 3rd ed. Newbury port: Prentice Hall; 1996.
17. Quigley, Morgan, etc. ROS: An open-source robot operating system. ICRA workshop on open source software 2009; 3(2).